ELSEVIER

Chemical Engineering Journal 117 (2006) 1–11

Chemical Engineering Journal

www.elsevier.com/locate/cej

Multi-scale modeling of gas–liquid–solid three-phase fluidized beds using the EMMS method

Guodong Jin *

Institute of Process Engineering, Chinese Academy of Sciences, P.O. 353, Beijing 100080, People's Republic of China

Received 20 March 2005; received in revised form 23 November 2005; accepted 7 December 2005

Abstract

A multi-scale model for the gas–liquid–solid three-phase fluidized beds is developed on the basis of the principles of the EMMS model. For this purpose, the flowing structure in the gas–liquid–solid system is divided into five phases and considered under different spatial scales: a solid–liquid phase describing the micro-scale interaction between solid particles and liquid, a gas phase, a bubble wake phase and two inter-phases that, respectively, describe the meso-scale interaction of the dispersed bubbles and bubble wakes with the surrounding liquid–solid pseudo-homogeneous suspension. In order to obtain the steady state of such a system with eight unknowns, in addition to seven mass and momentum conservation conditions and an inequality constraint for the mean bubble diameter, the stability condition $N_{st} \rightarrow \min$ is used.

The model is solved and checked with the experimental data available in several references which cover a broad range of operating conditions from the conventional expanded fluidized bed to the circulating fluidized bed, indicating that the model is capable of describing the global hydrodynamics of the complex flow in the three-phase system with acceptable accuracy.

Keywords: Gas–liquid–solid; Three-phase fluidization; Multi-scale method; EMMS model; Bubble diameter; Bubble wake

1. Introduction

In a typical gas–liquid–solid three-phase fluidized bed, solid particles are fluidized primarily by upward concurrent flow of liquid and gas, with liquid as the continuous phase and gas as dispersed bubbles if the superficial gas velocity is low. Because of the good heat and mass transfer characteristics, three-phase fluidized beds or slurry bubble columns ($u_t < 0.05$ m/s) have gained considerable importance in their application in physical, chemical, petrochemical, electrochemical and biochemical processing [1]. Intensive investigations have been performed on three-phase fluidization over the past few decades; however, there is still a lack of detailed physical understanding and predictive tools for proper design, scale-up and optimum operation of such reactors. The calculation of hydrodynamic parameters in these systems mainly relies on empirical correlations or semi-theoretical models such as the generalized wake model [2] and the structured wake model [1]. Though these models are capable of successfully elucidating the phenomena occurring in the three-phase reactors, too many parameters in them have limited their practical applications. In recent years, the computational fluid dynamics (CFD) based on the fundamental conservation equations has become a viable technique for process simulation [3–7]. Although powerful computer capability is available today, CFD is very expensive in terms of computer resources and time for full-scale, high-resolution, two- or three-dimensional simulation, and it is not readily applicable for routine design and scale-up of industrial-scale units, at least at present. Hence, there is a practical need to develop general and simple models for the three-phase fluidized beds.

Like the gas–solid fluidized systems, flows in the gas–liquid–solid three-phase fluidized beds are also characterized by structure heterogeneity and regime multiplicity due to the complex interactions between phases. For such complex systems, additional constraints for system stability may be indispensable in addition to those for mass and momentum conservation. On the other hand, gas–liquid–solid flow manifests its complex behavior largely at three different scales, i.e., micro-scale of solid particles, meso-scale of bubbles and bubble wakes, macro-scale of the whole bed unit with the influence of the unit boundary,

* Tel.: +86 1062659525; fax: +86 1062558065.
E-mail address: gd_jin@home.ipe.ac.cn.

1385-8947/$ – see front matter © 2005 Elsevier B.V. All rights reserved.
doi:10.1016/j.cej.2005.12.009

Nomenclature

b	width of the bubble (horizontal or major axis of the bubble)
$d_{3,2}$	Sauter mean bubble diameter determined by the maximum stable bubble theory (m)
d_b	mean bubble diameter (m)
Eo	Eötvös number, $Eo = g(\rho_m - \rho_g)d_b^2/\sigma$
E_{sur}	specific surface energy (J/m^3)
f_g	gas holdup
f_w	bubble wake holdup
k_0	mean relative size of the wake behind a single bubble (V_w/V_b)
Mo	Morton number, $Mo = g\mu_l^4(\rho_l - \rho_g)\rho_l^{-2}\sigma^{-3}$
N_d	power dissipated in particle collision, circulation, acceleration, liquid viscous dissipation with respect to unit mass of particles (J/(s kg))
N_{sur}	power consumed for increase of bubble surface energy with respect to unit mass of particles (J/(s kg))
N_{st}	power consumed for suspending and transporting unit mass of particles (J/(s kg))
N_T	total power consumed with respect to unit mass of particles (J/(s kg))
Re_b	gas Reynolds number with the characteristic length of bubble width, $Re_d = \rho_l b u_b \mu_l^{-1}$
Re_d	gas Reynolds number with the characteristic length of mean bubble diameter, $Re_d = \rho_l d_b u_b \mu_l^{-1}$
Re_g^*	modified gas Reynolds number, $Re_g^* = Re_l U_g / U_l$
Re_l	particle Reynolds number, $Re_l = \rho_l d_p U_l \mu_l^{-1}$
Ta	Tadaki number, $Ta = Re_d Mo^{0.25}$
u_b	bubble rising velocity (m/s)
$u_{b,i1}$	gas superficial velocity in inter-phase 1, $u_{b,i1} = u_b f_g/(1 - f_w)$
u_{dc}	particle superficial velocity in the liquid–solid mixture (m/s)
$u_{m,i1}$	liquid–solid suspension superficial velocity in inter-phase 1
$u_{m,i2}$	liquid–solid suspension superficial velocity in inter-phase 2
$u_{w,i2}$	bubble wake superficial velocity in inter-phase 2, $u_{b,i1} = u_b f_w/(1 - f_g)$
u_t	terminal velocity of a single particle in quiescent liquid (m/s)
U_d	solid superficial velocity (or particle circulating rate) (m/s)
U_g	gas superficial velocity (m/s)
U_l	liquid superficial velocity (m/s)
U_{lc}	liquid superficial velocity in the liquid–solid mixture (m/s)
W_{st}	power consumption for suspending and transporting in unit bed volume

Greek letters

ε_{lc}	liquid holdup in the liquid–solid mixture ($\varepsilon_{sc} = 1 - \varepsilon_{lc}$)
ε_{lw}	liquid holdup in the primary bubble wake ($\varepsilon_{sw} = 1 - \varepsilon_{lw}$)
ε_s	solid holdup, $\varepsilon_s = (1 - f_g - f_w)\varepsilon_{sc} + f_w\varepsilon_{sw}$
Λ	specific area (m^{-1})
ζ	local energy dissipation rate per unit mass of liquid

and interactions also occur among these different scales. Meanwhile, the multi-scale characteristic of turbulence induced by liquid shear and rising bubbles extremely complicates the system. Solid particles have complex interaction with turbulence eddies according to particle physical properties such as particle diameter and density. Turbulences at different scales have different effects on bubble behaviors, among which the turbulence at the length scale of bubble diameter is responsible for the bubble size. Therefore, effective analysis of the interactions at different spatial scales is especially important for appropriately describing the hydrodynamics in the three-phase flow.

The energy-minimization multi-scale (EMMS) method, originally developed for describing the gas–solid heterogeneous flow system by Li and Kwauk [8] and recently validated through discrete pseudo-particle approach [9], was extended to gas–liquid–solid three-phase flow system, however, without consideration of the effects of bubble wakes [10]. In fact, the hydrodynamics of bubble wake located immediately underneath the bubble base and rising at almost the same velocity of the bubble is totally different from that of the surrounding liquid–solid suspension. It has been specially recognized that the bubble wake is the dominating factor contributing to the intimate liquid/solid mixing and bed contraction performance [11]. In this study, the multi-scale resolution with respect to the scales of flowing structures in the three-phase flow is done with the consideration of the bubble wake effects. Simultaneously, the turbulent kinetic energy of the eddies induced by the rising bubbles and the surface energy are thought to be the dominating factors for controlling the bubble size.

2. EMMS model for three-phase fluidized beds

The EMMS model, effective for analyzing gas–solid two-phase fluidization [8], was generalized by Li and Kwauk [12]. It consists of the following main steps:

- Phenomenological resolution with respect to scales of structures.
- Establishment of conservation conditions with respect to different scales and correlation between different scales.
- Identification of dominant mechanisms and formulation of variational criterion to identify what dominates the stability of structure and what compromise exists between different dominant mechanisms.

- Integration between conservation conditions with stability conditions.

The EMMS model for the three-phase fluidized bed in this study is based on the above principles and the previous study on three-phase fluidized beds [10].

2.1. System resolution with respect to scales in three-phase system

Various interactions at different spatial scales occur in the gas–liquid–solid fluidized beds, including the persistent contacting of the particles and bubbles with liquid; and collisional interactions between bubbles and particles. The following analyses are based on the main interactions in the gas–liquid–solid fluidized beds.

Like the gas–solid two-phase system [8], the gas–liquid–solid system is resolved into a suspending and transporting subsystem and energy dissipation subsystem. Hence, the total power associated with a three-phase system, expressed as power consumed in a volume containing unit mass of solids, N_T, is considered to consist of the sum of the power for suspending and transporting particles, N_{st}, and the one purely dissipated in particle collision, circulation, acceleration, liquid viscous dissipation N_d, and the increase rate of surface energy due to bubble splitting N_{sur} ($N_T = N_{st} + N_d + N_{sur}$).

The overall flow behavior reflects the complex interactions among the individual phases at different scales. In order to efficiently describe the most prominent interaction of solid particles with liquid, and the interaction of rising gas bubbles and their wakes with the surrounding liquid–solid mixture, the suspending and transporting subsystem is further resolved into five phases: the liquid–solid phase, the gas phase, the bubble wake phase, one inter-phase describing the interaction between the rising gas bubbles and the surrounding liquid–solid suspension and the other inter-phase describing the interaction between bubble wakes and the surrounding liquid–solid suspension as shown in Fig. 1. Like the generalized bubble wake model [2], it is assumed that the wake rises at the same velocity as that of the bubble over it. Thus, eight variables are proposed to describe such systems, $\boldsymbol{X} = (f_g, f_w, u_b, u_{dc}, u_{lc}, \varepsilon_{lc}, \varepsilon_{lw}, d_b)$, where f_g is the holdup of the bubbles, f_w the holdup of bubble wakes, u_b the rising velocity of bubbles and bubble wakes, u_{dc} and u_{lc} the superficial velocity of particle and liquid in the solid–liquid phase, ε_{lc} the liquid holdup in the liquid–solid phase, ε_{lw} the liquid holdup in the bubble wake phase and d_b is mean bubble diameter.

As shown in Fig. 1, the interactions occurring in different phases are micro-scale of particles, meso-scale of bubbles and bubble wakes, and macro-scale of the whole bed unit, respectively. Micro-scale interaction is concerned with the interaction between individual particles and the fluid surrounding them. It is assumed that no particles are present in gas bubbles, and solid particles and liquid contained in a bubble wake rise at the same velocity as the bubble above it. Hence, micro-scale interaction only exists in the liquid–solid phase which is expressed as the balance between the drag force and effective gravity of solid particles. In the liquid–solid phase, the particles are assumed to be uniformly suspended, and the dilute–dense two-phase structure and thus the energy dissipation as in gas–solid system are neglected [8]. The interaction between particles and liquid in the liquid–solid phase can be described using the Richardson–Zaki relationship [13]. Meso-scale interactions are concerned with the interaction of dispersed bubbles and bubble wakes with the liquid–solid suspension. The former is expressed as the force acting on bubbles by the liquid–solid suspension through the inter-phase. The liquid–solid phase is treated as a pseudo-homogeneous mixture with the mean physical properties and averaged velocity. However, the interaction between bubble wakes and the liquid–solid phase is very complex, and it cannot be directly expressed with a simple theoretical relationship at present, thus the empirical correlations based on experiments are used to calculate the wake size and solid concentration in the primary wake. Macro-scale interaction occurs between the whole system and the boundaries such as the walls, the inlet and outlet of the bed. This macro-scale interaction will not be dealt with for the moment in this study.

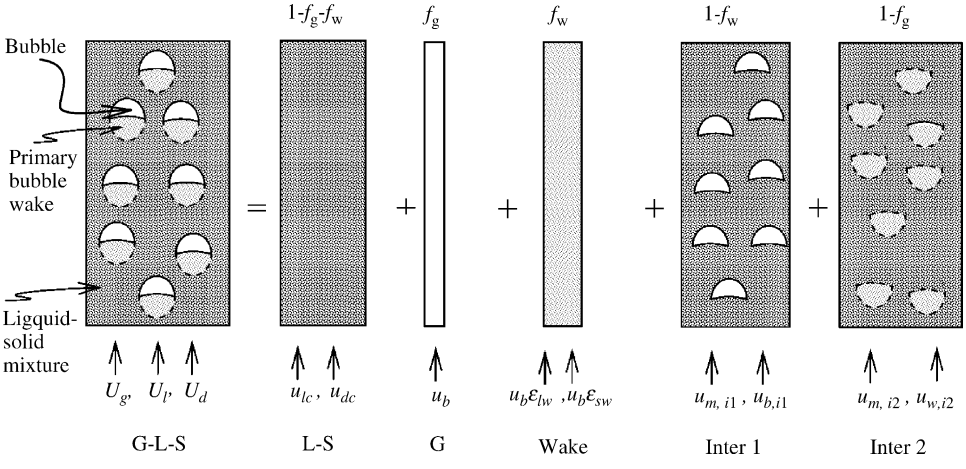

Fig. 1. Resolution for suspending and transporting subsystem in three-phase system based on different scales.

2.2. Conservation conditions at different scales

2.2.1. Momentum equation for particles in the liquid–solid phase

It is assumed that the generalized Richardson–Zaki relationship is suitable for the uniformly fluidized particles in the solid–liquid phase. This relationship implies the local balance among the gravity of particles, the buoyancy force and the drag force in unit volume of liquid–solid phase [14]:

$$\frac{u_{lc}}{\varepsilon_{lc}} - \frac{u_{dc}}{1-\varepsilon_{lc}} = u_t \varepsilon_{lc}^{n-1}, \tag{1}$$

where u_t is the terminal velocity of the particle in a stable liquid, and it can be iteratively computed using Eqs. (2)–(4) or obtained by experimental measurement [8],

$$u_t = \left(\frac{4gd_p(\rho_p - \rho_f)}{3\rho_f C_{D,p0}}\right)^{0.5}, \tag{2}$$

$$C_{D,p0} = \frac{24}{Re_t} + \frac{3.6}{Re_t^{0.313}}, \tag{3}$$

$$Re_t = \frac{\rho_l u_t d_p}{\mu_l}, \tag{4}$$

and n is Richardson–Zaki index, which depends on the terminal Reynolds number Re_t as follows [13]:

$$\begin{cases} n = 4.65 & Re_t < 0.2 \\ n = 4.4Re_t^{-0.03} & 0.2 < Re_t < 1 \\ n = 4.4Re_t^{-0.1} & 1 < Re_t < 500 \\ n = 2.4 & Re_t > 500 \end{cases}. \tag{5}$$

2.2.2. Momentum equation for dispersed bubbles in the liquid–solid suspension

Dispersed bubbles flow through the liquid–solid suspension which is regarded as a pseudo-homogeneous fluid with a mean density ρ_m, a mean superficial velocity u_m and an effective viscosity μ_m, which are, respectively, defined as [15]

$$\rho_m = \rho_p \varepsilon_{sc} + \rho_l \varepsilon_{lc}, \tag{6}$$

$$u_m = \frac{\rho_p u_{dc} + \rho_l u_{lc}}{\rho_m}, \tag{7}$$

$$\mu_m = \mu_l \exp\left(\frac{\varepsilon_{sc}}{1 - \varepsilon_{sc}/0.724}\right). \tag{8}$$

Bubbles interact with the mixture through the inter-phase 1 in which bubble wakes are not considered, thus the gas volume fraction is corrected as $f_g/(1-f_w)$ in this inter-phase. The efficient weight (the buoyancy minus weight) of bubbles in unit volume of inter-phase 1 is

$$\frac{f_g}{1-f_w}\left(\frac{1-f_w-f_g}{1-f_w}\rho_m + \frac{f_g}{1-f_w}\rho_g - \rho_g\right) g = \frac{f_g(1-f_w-f_g)}{(1-f_w)^2}(\rho_m - \rho_g)g. \tag{9}$$

The efficient weight is balanced by the drag force of the liquid–solid suspension, thus the momentum equation for bubbles can be expressed as

$$\frac{3}{4}\frac{1}{d_b}C_{D,b0}\left(1 - \frac{f_g}{1-f_w}\right)^m \rho_m \left(\frac{f_g}{1-f_w}\right)(u_b - u_m)^2 = \frac{f_g(1-f_w-f_g)}{(1-f_w)^2}(\rho_m - \rho_g)g, \tag{10}$$

where $C_{D,b0}$ is the drag coefficient for a single bubble and defined as [11]

$$C_{D,b0} = \max\left\{\left(\frac{24}{Re_d} + 3.6Re_d^{-0.313}\right), \frac{8}{3}\frac{Eo}{Eo+4}\right\}, \tag{11a}$$

or

$$C_{D,b0} = 2.7 + \frac{24}{Re_d}. \tag{11b}$$

Re_d is the Reynolds number with the characteristic length of the mean bubble diameter, $Re_d = \rho_m d_b (u_b - u_m)\mu_m^{-1}$ and Eo is Eötvös number which is defined as $Eo = g(\rho_m - \rho_g)d_b^2/\sigma$. $C_{D,g0}(1 - f_g/(1-f_w))^m$ is the drag coefficient for bubbles, including the effect of bubble swarm. m varies with the bubble terminal Reynolds number and $m = 2$ for large bubbles according to the drift model of Wallis [16].

2.2.3. Mean bubble wake size and particle concentration in the bubble wake

Turbulent bubble wake is unstable and the vortex in it sheds with a certain frequency. In order to quantify the extent of the exchange or interaction of the bubble wake phase with the surrounding liquid–solid mixture in inter-phase 2, two parameters, that is, the wake holdup, f_w (or the wake size) and the particle concentration in the wake ($\varepsilon_{sw} = 1 - \varepsilon_{lw}$) should be determined. Due to the instability of the wake, the wake size is not a constant but changes continuously with time as a saw-tooth wave function. It is very difficult to directly describe the interaction between the wake phase and surrounding liquid–solid phase theoretically, several models based on experimental observation or theoretical assumption, such as the saw-tooth wave function model, the bubble wake pendulum model, Hill's spherical model [11] and the completing spherical model [17] were proposed to compute the mean size of the bubble wake. In this study, the relationship combining two correlations for a steady wake behind a small bubble at low gas Reynolds numbers and for an unsteady wake at higher gas Reynolds numbers according to the saw-tooth wave function model is suggested to compute the mean relative size of the wake behind a single bubble ($k_0 = V_w/V_b$) in the three-phase fluidized beds [11],

$$k_0 = (200(Re_b - 20)^{-1.12} + 0.24)^{-1}. \tag{12}$$

Note that $Re_b = b\rho_m(u_b - u_m)\mu_m^{-1}$ and it is defined with a characteristic length of the major axis or width of the bubble b. It is more proper to define the gas Reynolds number due to the bubble shape transition apart from a sphere. To relate Re_b with Re_d, the ratio of equivalent diameter d_b to b, d_b/b and the aspect ratio (minor (vertical) axis/major (horizontal) axis) h/b should be

quantified. The aspect ratio is a function of the Tadaki number Ta, defined as $Ta = Re_d Mo^{0.25}$, and $Mo = g\mu_l^4(\rho_l - \rho_g)/(\rho_l^2\sigma^3)$. For three-dimensional system, this function is [18]

$$\frac{h}{b} = \begin{cases} 1 & Ta < 1 \\ (0.81 + 0.206\ \tanh(2(0.8 - \log_{10} Ta)))^3 & 1 < Ta < 39.8 \\ 0.24 & Ta > 39.8 \end{cases}. \quad (13)$$

For ellipsoidal and spherical-cap bubbles, $d_b/b = (h/b)^{1/3}$, thus

$$Re_b = Re_d \frac{b}{d_b}. \quad (14)$$

To account for the effect of gas holdup on bubble wake size, the volume fraction of bubble wake f_w can be expressed as

$$f_w = f_g k_0\ \exp(-5.05 f_g). \quad (15)$$

Solid concentration in the bubble wake increases with the decrease of particle size and the increase of gas velocity and liquid viscosity [17,19]. The empirical equation for the average solid holdup in the primary wake proposed by Kreischer et al. [19] can be used

$$\varepsilon_{sw} = 0.52\left(\frac{Re_d}{Re_t}\right)^{1/8} \varepsilon_{sc}^{5/4}. \quad (16)$$

2.2.4. Continuity equations for gas, liquid and solid

The continuity equations for gas, liquid and solid are, respectively,

$$u_b f_g - U_g = 0, \quad (17)$$

$$u_{lc}(1 - f_g - f_w) + u_b \varepsilon_{lw} f_w - U_l = 0, \quad (18)$$

$$u_{dc}(1 - f_g - f_w) + u_b(1 - \varepsilon_{lw}) f_w - U_d = 0. \quad (19)$$

2.3. Bubble size in three-phase fluidization

The multiple dispersed bubbles in the gas–liquid–solid system are thermodynamically unstable, however, can be maintained at a dispersed state with a mean bubble diameter due to the balance between the surface energy and the destructive turbulent kinetic energy input from the surrounding suspension. There exists a competitively dynamic process of bubble coalescence and break-up in three-phase fluidized beds.

For spherical bubbles with a given gas holdup in the three-phase system, the specific area $\Lambda = 6f_g/d_b$, and the specific surface energy $E_{sur} = \Lambda\sigma = 6\sigma f_g/d_b$. Bubble coalescence means the increase of d_b and the reducing of Λ, correspondingly, the reducing of the surface energy E_{sur}, bubble coalescence is thus a spontaneous tendency and the bubble diameter tends to become as large as possible through coalescence for a multiple-bubble system, leading to a minimum surface energy,

$$E_{sur} = \frac{6\sigma f_g}{d_b} \rightarrow E_{sur,min}. \quad (20)$$

Meanwhile, for a given gas holdup, larger bubbles suffer a smaller resistance when they go upwards through the liquid–solid mixture.

However, bubbles are dispersed and do not coalesce until two bubbles collide and contact for a certain period of time. In a three-phase fluidized bed, bubble coalescence may occur according to the mechanisms similar to those in a gas–liquid system. It is assumed that coalescence happens in three steps [20]: first, two bubbles collide, trapping a small amount of liquid as a thin film between them. Second, the liquid drains until the liquid film reaches a critical thickness. Third, the film ruptures, leading to the coalescence. Therefore, the coalescence rate is rated to two key parameters, that is, the collision rate and the collision efficiency. The collision rate may result from the large-scale turbulent eddies, the buoyancy and laminar shear. These mechanisms are cumulative. The collision efficiency is a measure of what fraction of bubble collisions lead to coalescence events, and it is a function of the contact time between bubbles and the time required for bubbles to coalesce [21].

On the other hand, the break-up of bubbles leads to the increase of specific area Λ, thus the increase of surface energy E_{sur}, additional work must be input from the surrounding suspensions. Few theories for bubble break-up in the three-phase fluidized bed are available. Except for the bubble-particle collision break-up mechanism [22], most of the theories for bubble break-up are derived from the theories proposed by Hinze [23] or Levich [24] for gas–liquid system. Large bubbles may be deformed and ruptured into smaller ones through bubble interaction with turbulent eddies generated in the liquid. The scale of eddies responsible for break-up is equal to or a little smaller than that of the bubble diameter. Large eddies just simply transport the bubbles, resulting in random motion of bubbles without causing them break up, while very small eddies do not contain sufficient energy to cause breakage. According to the theory of Hinze, the disruptive force acting on a bubble due to turbulent fluctuations is balanced by stabilizing surface tension. When the ratio of the two forces exceeds a critical Weber number value, the bubble breaks up,

$$We_c = \frac{\tau}{\sigma/d_{b,max}}, \quad (21)$$

where τ is the turbulent stress force of the liquid phase, $d_{b,max}$ the maximum stable bubble diameter and σ is the liquid–gas surface tension coefficient. Levich [24] postulates a similar force balance between the internal pressure of the bubble and surface tension of the deformed rather than the spherical bubble, to which the density of the dispersed bubble phase is introduced. The critical Weber number for Levich's theory can be simplified as

$$We_c' = \frac{\tau}{\sigma/d_{b,max}}\left(\frac{\rho_g}{\rho_l}\right)^{1/3}, \quad (22)$$

where ρ_l is the continuous liquid density and ρ_g is the dispersed gas density.

The turbulent stress force τ is characterized by Hinze as

$$\tau = \rho_l \overline{u'^2}, \tag{23}$$

where $\overline{u'^2}$ is the mean-square spatial fluctuation of liquid velocity, and it is related to the turbulence kinetic energy k in unit mass of liquid ($k = (3/2)\overline{u'^2}$ in isotropic and homogeneous turbulent flow) and $k \propto (l\zeta)^{2/3}$, l is the length scale of turbulence and ζ is the local energy dissipation rate per unit mass of liquid. Assuming the turbulence is isotropic and homogeneous in the gas dispersion region and taking the turbulence length scale l as $d_{b,max}$, Batchelor [25] related $\overline{u'^2}$ to ζ by

$$\overline{u'^2} \approx 2(\zeta d_{b,max})^{2/3}. \tag{24}$$

Introducing Eqs. (23) and (24) into Eq. (21), one can obtain the maximum stable bubble diameter according to Hinze's theory,

$$d_{max} = \left(\frac{We_c}{2}\right)^{0.6} \left(\frac{\sigma}{\rho_l}\right)^{0.6} \zeta^{-0.4}, \tag{25}$$

where the critical Webber number We'_c is in the range of 1.1–4.7. Similarly, introducing Eqs. (23) and (24) into Eq. (22), one can obtain the maximum stable bubble diameter according to Levich's theory,

$$d_{max} = \left(\frac{We'_c}{2}\right)^{0.6} \left(\frac{\sigma^{0.6}}{\rho_l^{0.4}\rho_g^{0.2}}\right) \zeta^{-0.4}, \tag{26}$$

where the critical Webber number We'_c is in the range of 0.6–1.5.

In practical application, the most commonly used bubble diameter is the Sauter mean diameter $d_{3,2}$, which measures the ratio of bubble volume to the surface area for a sample of N bubbles, and defined as

$$d_{3,2} = \frac{\sum_{i=1}^{N} n_i d_i^3}{\sum_{i=1}^{N} n_i d_i^2}. \tag{27}$$

The mean ratio of $d_{3,2}$ and $d_{b,max}$ is [26]

$$\frac{d_{3,2}}{d_{max}} = 0.62. \tag{28}$$

If the effect of the gas holdup on bubble size is considered, according to Levich's theory, the Sauter mean bubble diameter for the three-phase system can be expressed as [27]

$$d_{3,2} = 1.25 \left(\frac{\sigma^{0.6}}{\rho_m^{0.4}\rho_g^{0.2}}\right) \zeta^{-0.4} f_g^{0.37}, \tag{29}$$

where the local energy dissipation rate ζ is assumed to equate the rate of work done by the net buoyancy force acting on bubbles times the relative velocity of bubbles to the surrounding suspension in unit mass of liquid,

$$\zeta = \frac{1}{\varepsilon_l \rho_l} \frac{f_g(1 - f_w - f_g)(\rho_m - \rho_g)g}{(1 - f_w)^2}(u_b - u_m). \tag{30}$$

In gas–liquid–solid three-phase fluidized bed, the bubble-induced turbulence dominates over the liquid shear-induced turbulence over a broad operating range of gas superficial velocities [28]. Therefore, it is assumed that the mean size of bubbles is determined by the turbulent kinetic energy induced by the rising bubbles. The work done by the net buoyancy force of bubbles is first converted to the kinetic energy of eddies, that is, the turbulent kinetic energy in the primary wake required to maintain the vertical/circulating motion in the wake, and subsequently dissipated into the surrounding mixture as soon as part of the primary wake sheds into the secondary wake.

The maximum stable bubble diameter theory provides a constraint condition for the variation of mean bubble diameter:

$$d_b \le d_{3,2}. \tag{31}$$

The equation set including Eqs. (1), (10), (15)–(19) is the conservation conditions for the particles, bubbles and bubble wakes. The seven equations as well as the constraint condition (31) are not sufficient to determine the stable state of the gas–liquid–solid system with eight unknowns. Stability conditions for the three-phase system must be provided.

2.4. Stability conditions for three-phase fluidized beds

In the gas–liquid–solid fluidized bed, particles tend to maintain themselves as low as possible in the bed with minimum potential energy, leading to a maximal particle volume fraction $\varepsilon_s \to \varepsilon_{s,max}$. The continuous liquid directly contacts particles and its drag force balances the weight of the particles immersed it. The dispersed gas bubbles do not directly contact the particles except for particle–bubble collision; bubbles directly contact liquid and transfer their momentum to liquid to fluidize particles. The fluid motion tends to consume a minimum power for transporting and suspending particles per unit bed volume, that is, $W_{st} = W_{st,l-s} + W_{st,gas} \to W_{st,min}$. In most flow regimes, neither the particles nor the fluid can dominate the other in displaying either's tendency exclusively, they have to compromise each other in such as way that the particles seek as much as possible minimum potential energy and the fluids (including continuous liquid and dispersed bubbles) flow through the particles as much as possible with minimum resistance, leading to the stability condition for the three-phase fluidized beds, the same as the gas–solid two-phase flow [8]:

$$N_{st} = N_{st,l-s} + N_{st,gas} \to N_{st,min}, \tag{32}$$

where N_{st} is defined as the power consumed for transporting and suspending particles in a volume containing unit mass of particles, $N_{st} = W_{st}/(\varepsilon_s \rho_p)$. The associated correlations for N_{st} are listed in Table 1.

2.5. Summary of the EMMS model for three-phase fluidized beds

Integrating the constraint conditions with the stability condition, one can get the EMMS model for the gas–liquid–solid three-phase fluidized bed, which is an optimization problem with an objective function $N_{st} \to N_{st,min}$ and seven equality constraints for mass and momentum conservation (Eqs. (1), (10),

Table 1
Correlations in the EMMS model for three-phase fluidized bed

	Liquid–solid phase	Bubble/liquid–solid suspension
Slip velocity	$u_{sc} = \frac{u_{lc}}{\varepsilon_{lc}} - \frac{u_{dc}}{\varepsilon_{sc}}$	$u_{sb} = u_b - u_m$
Drag coefficient for single bubble		$C_{D,b0} = \max\left\{\left(\frac{24}{Re_d} + \frac{3.6}{Re_d^{0.313}}\right), \frac{8}{3}\frac{Eo}{Eo+4}\right\}$
Drag coefficient for bubble swarm		$C_{D,b} = C_{D,b0}\left(1 - \frac{f_g}{1-f_w}\right)^2$
Momentum exchange coefficient	$\beta_{lc} = \frac{(\rho_p-\rho_l)g\varepsilon_{sc}\varepsilon_{lc}^{2-n}}{u_t}$	$\beta_{int1} = \frac{3}{4}\frac{C_{D,b}\rho_m}{d_b}\left(\frac{f_g}{1-f_w}\right)(u_b - u_m)$
Drag force for particles or bubbles in unit volume	$F_{dp} = \beta_{sc}u_{sc}$	$F_{dp} = \beta_{int1}u_{sb}$
Suspending and transporting power consumed in unit volume	$W_{st,l-s} = F_{dp}u_{lc}$	$W_{st,gas} = \frac{F_{dg}u_g}{1-f_w}$
Volume containing unit mass of particles	$\frac{1}{\varepsilon_s\rho_p} = \frac{1}{\rho_p((1-f_g-f_w)\varepsilon_{sc}+f_w\varepsilon_{sw})}$	
Suspending and transporting power consumed per unit mass of particles	$N_{st,l-s} = \frac{W_{st,l-s}(1-f_g-f_w)}{\varepsilon_s\rho_p}$	$N_{st,gas} = \frac{W_{st,gas}(1-f_w)}{\varepsilon_s\rho_p}$

(15)–(19)) as well as an inequality constraint for bubble diameter (Eq. (31)).

3. Model solution and optimal solution

If we select one of the eight unknowns and give it a trial value in a proper range, for example, f_g in the open interval (0, 1), the seven equations is closed for the other seven unknowns. For every given trial value of f_g, we can solve the non-linear equation set established in the above section iteratively, and if the solution exists, we can compute the value of objective function N_{st}. Through this method, we can know the variational tendencies of all the parameters, as well as the objective function, and search the optimal solution among all the feasible solutions.

Fig. 2 shows the feasible solutions and optimal solution of a gas–liquid–solid three-phase fluidized bed. The physical properties of the gas, liquid, solid and the operating conditions used are the system 1 listed in Table 2 with $Re_g^* = 40$ and $Re_l = 101$. Fig. 2(a and b) are the feasible solutions of d_b and ε_s ($\varepsilon_s = (1 - f_g - f_w)\varepsilon_{sc} + f_w\varepsilon_{sw}$), and Fig. 2(c and d) are the variation tendencies of the objective function N_{st} and specific surface energy E_{sur} when the gas holdup varies from 0.12 to 0.1 from right to left, where the dash line in Fig. 2(a) is the Sauter mean diameter determined from the maximum stable bubble theory, Eq. (29) and the solid line is the mean bubble diameter obtained from the conservation equation set. When f_g varies from 0.12 to 0.1, from right to left, d_b is less than the maximum stable Sauter mean diameter, bubble tends to coalesce and d_b increases, the specific area Λ and the surface energy E_{sur} thus decreases. At the same time, N_{st} decreases with the increase of solid holdup ε_s. Therefore, the gas–liquid–solid system tends to be stable. At the point A, the solid line intersects with the dash line, and d_b equates the maximum stable Sauter mean diameter, indicating the balance of bubble coalescence and break-up, and meanwhile, the objective function reaches its minimum extremum in the possible range. From point A to left, the mean bubble diameter obtained from the conservation equation set is greater than the Sauter mean diameter obtained from the maximum stable bubble theory and that does not occur in reality. Therefore, the optimal solution is at point A and $f_g = 0.102$, $\varepsilon_s = 0.326$ and $d_b = 0.0063$ m.

4. Model solution and validation

In this section, we solve and validate the EMMS model for three-phase fluidized beds using the experimental data available in several references which cover a broad range of operating conditions from the conventional expanded bed to the circulating fluidized bed.

4.1. Conventional expanded bed

Macchi et al. [29] have carried out experiments in two gas–liquid–solid systems: an aqueous glycerol solution with glass beads (system 1) and silicone oil with porous alumina particles (system 2), with air as the gas phase in both cases. The physical properties of the materials used and the operating conditions are listed in Table 2. The hydrodynamic similitude is met in the two systems, according to the following five dimensionless groups [30]:

$$Mo = \frac{g(\rho_l - \rho_g)\mu_l^4}{\rho_l\sigma^3}, \quad Eo = \frac{g(\rho_l - \rho_g)d_p^2}{\sigma},$$
$$Re_l = \frac{\rho_l d_p U_l}{\mu_l}, \quad \frac{\rho_p}{\rho_l}, \quad \frac{U_g}{U_l}. \tag{33}$$

Table 2
The physical properties of the materials and operating conditions used in Ref. [29]

	μ_l (Pa s)	σ (N/m)	ρ_l (kg/m^3)	ρ_p (kg/m^3)	ρ_g (kg/m^3)	d_p (m)	ε_{smf}	h_0 (m)	U_g (m/s)	U_l (m/s)
System 1	0.0068	0.067	1128	2230	1.2	0.006	0.58	0.52	0–0.06	0.1015
System 2	0.0024	0.0178	953	1881	1.2	0.0032	0.58	0.52	0–0.047	0.08

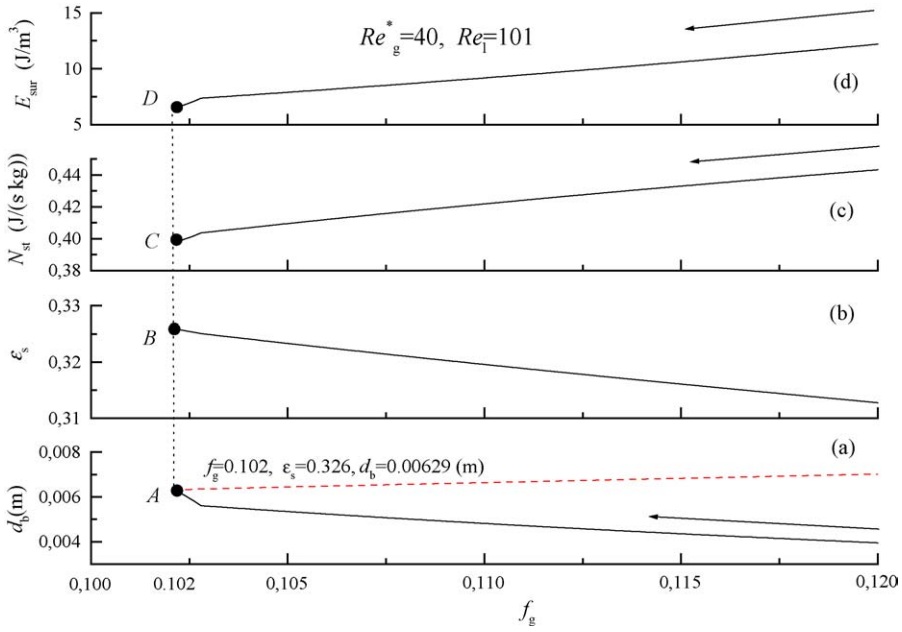

Fig. 2. Feasible and optimal solutions of EMMS model for gas–liquid–solid three-phase flow.

Fig. 3 shows the gas holdup versus the modified gas Reynolds number $Re^*_g = Re_l U_g / U_l$ at $Re_l = 101$. The gas holdup increases with the increase of Re^*_g in the dispersed bubble regime and the prediction results well fit the experimental data.

The bed expansion versus Re^*_g is plotted in Fig. 4 for the two systems at $Re_l = 101$. The prediction results show that when gas is first introduced with a small velocity, the bed height collapses rather than expands due to the bubble wake effect. This may result from two facts. One is that the bubble drags a portion of liquid in the wake out of the bed surface when it comes out of the bed, making the bed height decrease; the other is the change of the hydrodynamics because of the introduction of gas into the bed. At the beginning, gas enters the bed and occupies only a very little volume; it soon gets a velocity due to the buoyancy, inducing a portion of liquid in the wake to rise at the same speed which is faster than that of the surrounding liquid. The rising liquid in the bubble wake makes the surrounding liquid slow down according to the liquid phase continuity equation (Eq. (18)). Once the surrounding liquid velocity decreases, the particles begin to descend according to Eq. (1), making the bed collapse. At higher gas superficial velocities with the increase of gas holdup, the bed height begins to expand. As the experiments were carried out in the high gas velocity region, $Re^*_g > 20$, the bed collapse phenomenon was not reported in Ref. [29].

4.2. Gas–liquid–solid circulating fluidized bed

Liang et al. [31] and Yang et al. [32] have studied the hydrodynamics and gas–liquid interfacial area in a three-phase fluidized bed using the tap water and air as the liquid and gas phases, respectively, and glass beads as the solid phase in a column with

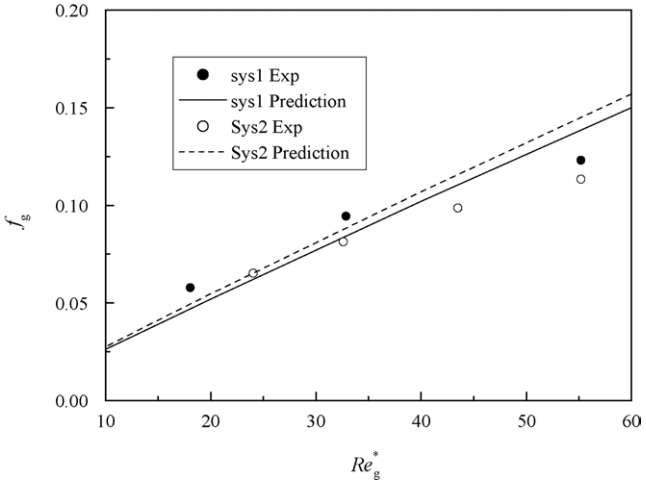

Fig. 3. Gas holdup vs. Re^*_g at $Re_l = 101$.

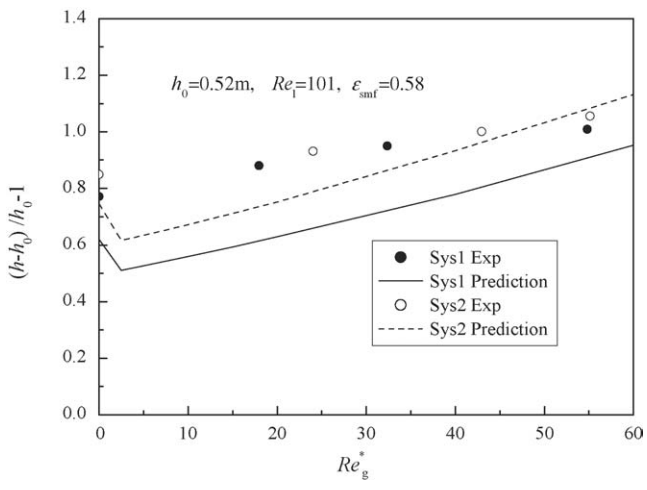

Fig. 4. Bed expansion vs. Re^*_g at $Re_l = 101$.

Table 3
The physical properties of the materials used in Refs. [31,32]

μ_l (Pa s)	0.001
σ (N/m)	0.072
ρ_l (kg/m^3)	1000
ρ_p (kg/m^3)	2460
ρ_g (kg/m^3)	1.18
d_p (m)	0.0004

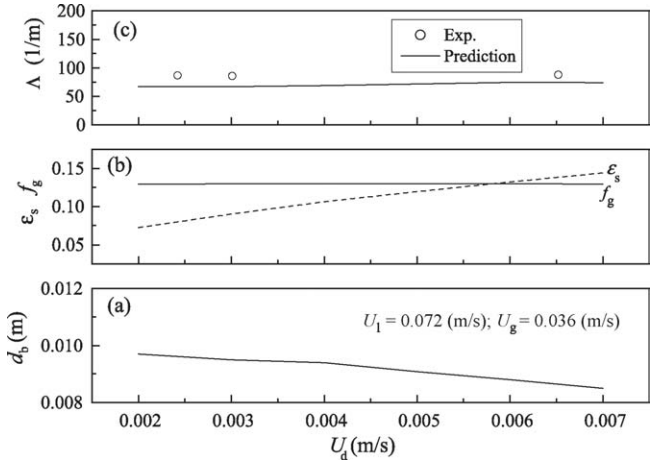

Fig. 5. The effect of particle circulating rate on the bubble diameter, gas and solid holdup and gas–liquid specific area.

0.14 m in i.d. and 3.0 m in height. The physical properties of the materials used are listed in Table 3.

Fig. 5 shows the effect of particle circulating rate U_d on the bubble diameter, gas and solid holdup and gas–liquid specific area. Solid holdup increases with the increase of particle circulating rate, while bubble diameter decreases a little and gas holdup almost keeps a constant. Fig. 5(c) shows the comparison between the experimental results and prediction on gas–liquid specific area [32].

Fig. 6 shows the comparison between the experimental and prediction results on solid holdup variation with the liquid velocity [31]. The prediction underestimates the solid holdup a little

Table 4
The physical properties of the materials and operating conditions used in Ref. [33]

μ_l (Pa s)	0.001
σ (N/m)	0.072
ρ_l (kg/m^3)	1000
ρ_p (kg/m^3)	2250
ρ_g (kg/m^3)	1.18
d_p (m)	0.0013
G_s (kg/m^2 s)	14.2
U_g ($\times 10^2$ m/s)	0.329
	0.786
	1.645
U_l (m/s)	0.142

under the operating conditions, however, within an acceptable accuracy considering the complexity of the three-phase flow.

Liu et al. [33] have experimentally studied the hydrodynamics in gas–liquid–solid three-phase flow in a Plexiglas circulating fluidized bed with a riser 0.076 m in i.d. and 2 m in height and a downer of 100 mm in i.d. Air and tap water were used as the gas and liquid phase, respectively, and glass beads were employed as the solid phase. The physical property of these materials and the operating conditions are listed in Table 4.

Fig. 7 shows the comparison between the experimental and the prediction results about the gas, liquid and solid holdup with the variation of gas superficial velocity U_g at the bed height of 1.2 m where the flow is fully developed, the data are the cross-sectional averaged value of the measurement data in different radial points. The fitness of the two results is quite good. Fig. 8 shows the holdup of gas, solid, bubble wake and the solid concentration in the bubble wake with the variation of U_g. Gas and bubble wake holdup increase with the increase of U_g, and the solid holdup increases a little at low gas velocities due to the bubble wake effects and decreases with the further increase of U_g (see the inset with an enlarged scale), while the solid concentration in bubble wake increases a little and almost keeps a constant with the increase of U_g under the experimental conditions.

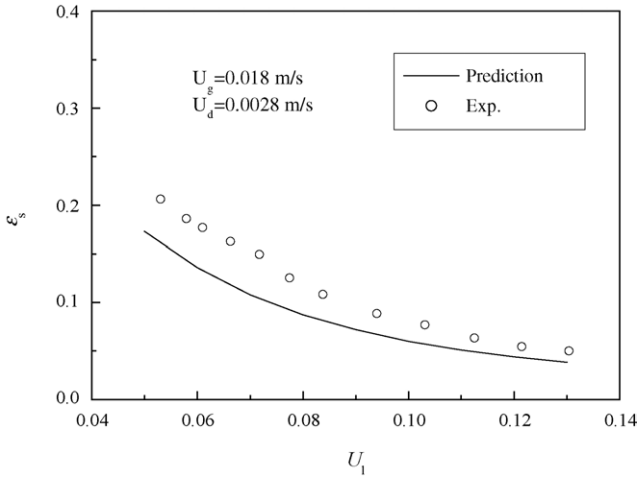

Fig. 6. Solid holdup under different liquid velocities.

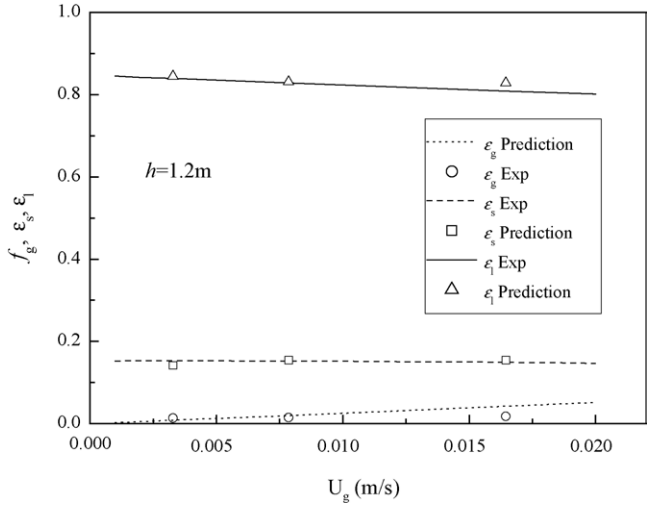

Fig. 7. Gas, liquid and solid holdup variation with U_g.

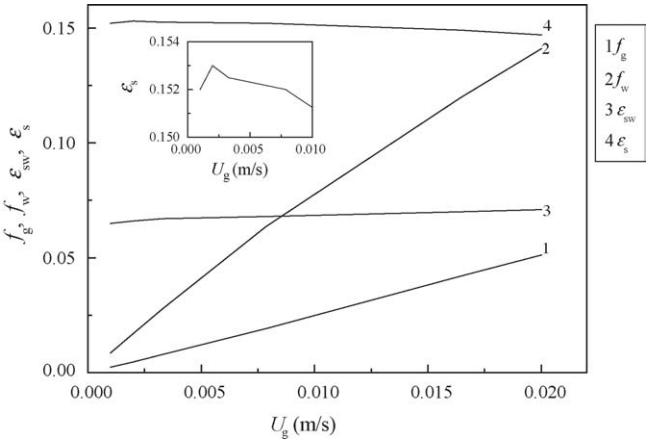

Fig. 8. Gas, solid, bubble wake holdup and solid concentration in bubble wake variation with U_g.

5. Conclusions

(1) A multi-scale model for the gas–liquid–solid three-phase fluidized bed based on the principles of the EMMS model is developed with the consideration of the bubble wake effects. For this purpose, the suspending and transporting subsystem is revolved into five phases, eight unknowns are proposed to describe such a system, conservation relationships are established under different spatial scales, bubble diameter is constrained by a critical value, $d_{3,2}$, obtained from the maximum stable bubble diameter theory, which means the surface energy of the bubbles is balanced by the turbulent kinetic energy of the liquid under a length-scale of bubble diameter induced by the rising bubbles. In order to obtain the steady state, the stability condition $N_{st} = W_{st}/(\varepsilon_s \rho_p) \rightarrow N_{st,min}$ is used, which means the compromise of the tendency of particles to maintain a minimum potential energy ($\varepsilon_s \rightarrow \varepsilon_{s,max}$) and the tendency of liquid and gas to consume a minimum power to suspend and transport the particles in the bed ($W_{st} = W_{st,l–s} + W_{st,gas} \rightarrow W_{st,min}$).

(2) The EMMS model for three-phase fluidized bed is an optimization problem, with an objective function ($N_{st} \rightarrow$ min) subject to seven equality constraints for mass and momentum conservation and an inequality constraint for the mean bubble diameter.

(3) Solved and validated by the experimental data available from several references covering a broad range of operating conditions, the EMMS model established in this study is capable of describing the global hydrodynamics of gas–liquid–solid three-phase fluidized bed with acceptable accuracy. The unique bed contraction–expansion phenomenon occurring in the three-phase system can also be predicted.

Acknowledgements

The financial support from the National Nature Science Foundation of China (Nos. 20490201 and 20221603) and China Postdoctoral Science Foundation (No. 2003034918) is gratefully acknowledged. The author would like to express his thanks to Professor Jinghai Li for the guidance and support in carrying out this study.

References

[1] L.-S. Fan, Gas–Liquid–Solid Fluidization Engineering, Butterworth-Heinemann, Boston, 1989.
[2] V.K. Bhatia, N. Epstein, Three-phase fluidization: a generalized wake model, in: H. Angelino, J.P. Couderc, H. Gibert, H. Lagueric (Eds.), Proceedings of the International Symposium on Fluidization, Its Application, Cepadues-Editions, Toulouse, 1974, pp. 380–392.
[3] D. Mitra-majumdar, B. Farouk, Y.T. Shah, Hydrodynamics modeling of three-phase flows through a vertical column, Chem. Eng. Sci. 52 (1997) 4485–4497.
[4] Y. Li, J. Zhang, L.-S. Fan, Numerical simulation of gas–liquid–solid fluidization systems using a combined CFD-VOF-DPM method: bubble wake behavior, Chem. Eng. Sci. 54 (1999) 5101–5107.
[5] R.S. Oey, R.F. Mudde, L.M. Portela, H.E.A. van den Akker, Simulation of a slurry airlift using a two-fluid model, Chem. Eng. Sci. 56 (2001) 673–681.
[6] D. Matonis, D. Gidaspow, M. Bahary, CFD simulation of flow and turbulence in slurry bubble column, AIChE J. 48 (2002) 1413–1429.
[7] I.K. Gamwo, J.S. Halow, D. Gidaspow, R. Mostofi, CFD models for methanol synthesis three-phase reactors: reactor optimization, Chem. Eng. Sci. 93 (2003) 103–112.
[8] J.H. Li, M. Kwauk, Particle–Fluid Two-Phase Flow—Energy-Minimization Multi-Scale Method, Metallurgical Industry Press, Beijing, 1994.
[9] J.Y. Zhang, W. Ge, J.H. Li, Simulation of heterogeneous structures and analysis of energy consumption in particle–fluid system with pseudo-particle modeling, Chem. Eng. Sci. 60 (2005) 3091–3099.
[10] M.Y. Liu, J.H. Li, M. Kwauk, Application of the energy-minimization multi-scale method to gas–liquid–solid fluidized beds, Chem. Eng. Sci. 56 (2001) 6805–6812.
[11] L.-S. Fan, K. Tsuchiya, Bubble Wake Dynamics in Liquid and Liquid–Solid Suspensions, Butterworth-Heinemann, Boston, 1990.
[12] J.H. Li, M. Kwauk, Exploring complex systems in chemical engineering—the multi-scale methodology, Chem. Eng. Sci. 58 (2003) 521–535.
[13] J.F. Richardson, W.N. Zaki, Sedimentation and fluidization: part 1, Trans. Inst. Chem. Eng. 32 (1954) 35–53.
[14] G.D. Jin, D.Y. Liu, Modeling and simulation of liquid pulsed particulate fluidized beds, Powder Technol. 152 (2005) 138–155.
[15] K. Tsuchiay, A. Furumoto, L.-S. Fan, J.P. Zhang, Suspension viscosity and bubble rise velocity in liquid–solid fluidized bed, Chem. Eng. Sci. 52 (1997) 3053–3066.
[16] G.B. Wallis, One-Dimensional Two-Phase Flow, McGraw-Hill Inc., 1969.
[17] S.A. El-Temtamy, N. Epstein, Bubble wake content in three-phase fluidized beds, Int. J. Multiphase Flow 4 (1978) 19–31.
[18] R. Clift, J.R. Grace, M.E. Weber, Bubbles, Drops and Particles, Academic Press, New York, 1978.
[19] B.E. Kreischer, H. Moritomi, L.-S. Fan, Wake solids holdup characteristics behind a single bubble in three-dimensional liquid–solid fluidized bed, Int. J. Multiphase Flow 16 (1990) 187–200.
[20] M.J. Prince, H.W. Blanch, Bubble coalescence and break-up in air-sparged bubble columns, AIChE J. 36 (1990) 1485–1499.
[21] C.A. Coulaloglou, L.L. Tavlarides, Description of interaction process in agitated liquid–liquid dispersion, Chem. Eng. Sci. 32 (1977) 1289–1297.
[22] Y.M. Chen, L.-S. Fan, Bubble breakage mechanisms due to collision with a particle in a liquid medium, Chem. Eng. Sci. 44 (1989) 117–132.
[23] J.O. Hinze, Fundamentals of the hydrodynamic mechanism of splitting dispersion process, AIChE J. 1 (1955) 289–295.
[24] V.G. Levich, Physiochemical Hydrodynamics, Prentice Hall, Englewood Cliff, NJ, 1962.

[25] G.B. Batchelor, Theory of Homogeneous Turbulence, Cambridge University Press, Cambridge, 1956.
[26] R.P. Hesketh, T.W. Fraser Russell, A.W. Etchells, Bubble size in horizontal pipelines, AIChE J. 33 (1987) 663–667.
[27] V.P. Metkin, V.N. Sokolov, Effect of the gas content on bubble sizes in gas–liquid systems, Zhurnal Prikladnoi Khimii 58 (1985) 1132–1134.
[28] Z. Cui, L.-S. Fan, Turbulence energy distributions in bubbling gas–liquid and gas–liquid–solid flow systems, Chem. Eng. Sci. 59 (2004) 1755–1766.
[29] A. Macchi, H.T. Bi, J.R. Grace, C.A. McKnight, L. Hackman, Dimensional hydrodynamic similitude in three-phase fluidized beds, Chem. Eng. Sci. 56 (2001) 6039–6045.
[30] M. Safoniuk, J.R. Grace, L. Hackman, C.A. McKnight, Use of dimensional similitude for scale-up of hydrodynamics in three-phase fluidized beds, Chem. Eng. Sci. 54 (1999) 4961–4966.
[31] W. Liang, Q. Wu, Z. Yu, Y. Jin, Z. Wang, Hydrodynamics of gas–liquid–solid three-phase circulating fluidized bed, Can. J. Chem. Eng. 73 (1995) 656–661.
[32] W.G. Yang, J.F. Wang, T.F. Wang, Y. Jin, Experimental study on gas–liquid interfacial area and mass transfer coefficient in three-phase circulating fluidized beds, Chem. Eng. J. 84 (2001) 485–490.
[33] Z.L. Liu, M. Vatanakul, L.F. Jia, Y. Zheng, Hydrodynamics and mass transfer in gas–liquid–solid circulating fluidized beds, Chem. Eng. Technol. 26 (2003) 1247–1253.